# First-principles study of nickel reactivity under two-dimensional cover:
# Ni$_2$C formation at rotated graphene/Ni(111) interface

Srdjan Stavrić [1,2,*] Simone del Puppo [1] Željko Šljivančanin [2] and Maria Peressi [1]

[1]*Physics Department, University of Trieste, via A. Valerio 2, Trieste 34127, Italy*
[2]*Vinča Institute of Nuclear Sciences - National Institute of the Republic of Serbia, University of Belgrade,*
*P. O. Box 522, RS-11001 Belgrade, Serbia*

Recent experiments indicate that the reactivity of metal surfaces changes profoundly when they are covered with two-dimensional (2D) materials. Nickel, the widespread catalyst choice for graphene (G) growth, exhibits complex surface restructuring even after the G sheet is fully grown. In particular, due to excess carbon segregation from bulk nickel to surface upon cooling, a nickel carbide (Ni$_2$C) phase is detected under rotated graphene (RG) but not under epitaxial graphene (EG). Motivated by this experimental evidence, we construct different G/Ni(111) interface models accounting for the two types of G domains. Then, by applying density functional theory, we illuminate the microscopic mechanisms governing the structural changes of nickel surface induced by carbon segregation. A high concentration of subsurface carbon reduces the structural stability of Ni(111) surface and gives rise to the formation of thermodynamically advantageous Ni$_2$C monolayer. We show the restructuring of the nickel surface under RG cover and reveal the essential role of G rotation in enabling high density of favorable C binding sites in the Ni(111) subsurface. As opposed to RG, the EG cover locks the majority of favorable C binding sites preventing the build-up of subsurface carbon density to a phase transition threshold. Therefore we confirm that the conversion of C-rich Ni surface to Ni$_2$C takes place exclusively under RG cover, in line with the strong experimental evidence.

## I. INTRODUCTION

Since the modern debut of graphene (G) in 2004 [1,2] this first genuinely two-dimensional (2D) crystal continues to exhibit scientific and technological promise across various disciplines. To achieve the full potential in nanotechnology, the efficient and cheap methods for producing large flakes of high-quality graphene must be matured. Among presently available techniques aimed towards fulfilling this goal, one of the most promising is chemical vapor deposition (CVD), widely used to grow graphene from carbon atoms of gaseous hydrocarbons deposited on transition metal surfaces [3,4].

The CVD growth of high-quality graphene largely depends on the properties of the support. Ni(111) surface is a widespread choice, due to close lattice match with G and the ease of dehydrogenation of precursor hydrocarbons [5–7]. On the other hand, at variance with other transition metal surfaces, the Ni(111) surface becomes unstable upon exposure to hydrocarbons and undergoes the "clock reconstruction", which leads to the formation of highly stable nickel carbide (Ni$_2$C) phase [8–10]. This structural phase transition opens new possibility to grow G not directly from decomposed hydrocarbons but from the precursor carbide, that is in a second step converted into G [11,12]. Besides G domains aligned with the nickel surface (EG), with the appropriate substrate

pre-treatment and the suitable choice of the CVD parameters, rotated domains (RG) can also be observed [12].

The interplay between carbide and graphene is not limited to the G growth process. Even in a presence of a complete G monolayer on top of Ni(111) surface, carbide structures are experimentally detected under G layer, irrespective of its specific growth mechanism. Intriguingly, such carbide domains, emerged upon segregation of dissolved carbon during the cooling of the sample, are found solely under RG domains [12]. Even more captivating is the experimental demonstration of reversible carbide formation/dissolution through the control of temperature [13]. As an aftermath, this manipulation results in switching of graphene electronic structure from semimetallic to metallic and vice versa. In particular, the presence of carbide under the G sheet considerably affects its electronic properties, as the increase of G distance from the substrate by $\sim$1 Å drastically weakens the graphene-nickel interaction and restores G's semi-metallic nature. The relevance of this reversible process in the design of controllable graphene/metal interfaces underlines the necessity for a better understanding of the reactivity of metal surface covered by 2D materials. However, the microscopic mechanism that leads to the formation of carbide under the rotated G but hinders its formation under epitaxial G is still under debate.

In the present study, we focus on Ni$_2$C formed under G layer. Given that the environment under 2D cover is not easily monitored by low-energy electron diffraction (LEED) analysis or scanning tunneling microscopy (STM), we performed DFT calculation to gain additional insights on the

*sstavric@units.it

atomic structure and the reactivity of metal surfaces under G cover. Concretely, we investigated the combined effects of atomic carbon intercalants at G/Ni(111) interface and of G rotation on the $Ni_2C$ formation. It turns out that C atoms bound in Ni(111) under G trigger profound structural changes in a metal layer near the surface. Ab-initio calculations shed light on the origin of $Ni_2C$ formation, while the atomistic picture constructed from the obtained results complements the evidence from experiments.

We start with the description of the applied computational methodology in Sec. II. The results presented in Sec. III are organized as follows: the structural and electronic properties of G epitaxially aligned and rotated at $Ni_2C$/Ni(111) substrate, EGC and RGC heterostructures, are examined in Sec. III A; the microscopic mechanisms behind the formation of carbide under G cover and the importance of G misalignment with nickel surface for this phase transition are inspected in Sec. III B. The main results are summarized in Sec. IV.

## II. COMPUTATIONAL DETAILS

First-principles calculations were carried out in the framework of spin-polarized DFT calculations using QUANTUM ESPRESSO package [14,15], based on plane waves and pseudopotentials. The effects of the exchange and correlation (XC) in the electronic gas were taken into account by means of Perdew-Burke-Ernzerhof (PBE) parametrization form within generalized gradient approximation (GGA) [16]. Due to an essential role of van der Waals (vdW) forces in proper description of the interaction between the graphene and the nickel surfaces, the dispersive corrections to the XC functional were employed within the semiempirical vdW-DF2 scheme [18].

The electron wave functions and the electron density were expanded in plane waves basis sets with cutoff energies of 30 and 200 Ry, respectively. The convergence threshold for total energy in all calculations was set to $1.0 \times 10^{-6}$ Ry. In order to calculate core-level shifts of C 1*s* states in different carbon species, we constructed the ultrasoft pseudopotential with one missing C 1*s* core electron using the ld1.x atomic code of QUANTUM ESPRESSO package within the scalar-relativistic approximation. The thorough testing is performed to assure that the pseudopotential displays good transferability. According to test results, provided in Ref. [17], in all calculations involving this pseudopotential the plane wave cutoffs of the wave function and electron density expansions are increased to 50 and 250 Ry, respectively.

To model the Ni(111) surface we used the lattice parameter of 3.52 Å, similar to the values reported in literature obtained with PBE XC functional [19]. The G/Ni(111) structures, EG and RG, are modeled using a hexagonal unit cell with lateral size of 10.8 Å. The G/$Ni_2C$/Ni(111) heterostructures, EGC and RGC, are modeled with monoclinic cell with lateral sizes of 14.9 and 16.3 Å. The thickness of vacuum region in both cases is set to at least 13 Å. During the structural relaxations, the Brillouin-zone (BZ) integration has been performed with 4 **k** points using the smearing special-point technique [20,21] and a smearing parameter of 0.01 Ry. All atoms but those in the bottom Ni layer were allowed to relax until the forces were smaller than 0.001 Ry/Bohr. Upon reaching the structural equilibrium, further self-consistent calculations with fixed

atomic positions were performed with 16 **k** points in the BZ. The non-self-consistent calculations with fixed potential needed for the computation of total and atom-projected density of states (DOS) were performed with 100 **k** points in the BZ. Energy barriers in the segregation process of C atom were calculated by means of the nudged elastic band (NEB) method with the quasi-Newton Broyden optimization scheme employed. The path was discretized into eight images and the simulations were stopped when the norm of the force orthogonal to the path was less than 0.1 eV/Å. We used the Atomic Simulation Environment (ASE) [22,23] for modeling and displaying the structures and XCRYSDEN [24] for plotting the induced charge density (ICD).

## III. RESULTS AND DISCUSSION

### A. G/$Ni_2C$/Ni(111) heterostructures

We introduce two models of G at $Ni_2C$/Ni(111) substrate—EGC, where G is epitaxially aligned with nickel, and RGC, where the angle between G zigzag direction and $\langle 110 \rangle$ direction of Ni(111) surface is $\sim 16°$. The stability of two heterostructures is carefully examined by thermodynamic arguments. After the models are tested by comparing the DFT-calculated C 1*s* core-level shifts with the measurements, we reveal the influence of carbide on the electronic properties of G cover.

#### 1. Structural models of G at $Ni_2C$/Ni(111) substrate

Common hexagonal crystal structure and small lattice mismatch allow graphene to perfectly align on top of Ni(111) without moirée pattern or substantial tension. Being aligned on Ni(111), the sublattices of graphene can adopt a few different adsorption sites, giving rise to several EG structures very close in energy [25,26]. The ambiguity of EG structure is thoroughly examined by both theoretical and experimental approaches with the conclusions drawn (1) that the vdW forces are essential for the stability of G on Ni(111) and thus must be included in DFT calculations [27,28] and (2) that EG structures with different G adsorption configurations can coexist in experimental conditions due to kinetic factors present during the growth [26,29]. Using DFT-GGA calculations with semiempirical vdW-DF2 long-range dispersive corrections, Sun *et al.* reported that top-fcc is energetically the most favorable geometry, followed by top-bridge, top-hcp, and hcp-fcc [30]. Similar results are reported by Bianchini *et al.* [26]. Bearing in mind that our computational approach is comparable to that applied in Refs. [26,30], we modeled the EG structure with G adsorbed in the top-fcc configuration. This choice is further corroborated by experimental findings [26,31,32]. The relevance of the particular G adsorption configuration for the stability of EG will be discussed in detail in Sec. III B.

In experimental studies on G/Ni(111) interface, the fingerprints of the post-growth carbide are found solely under rotated graphene (RGC domains) [12,13]. Moreover, combined LEED analysis and STM imaging on RGC domains showed a variety of G rotation angles [11], while further studies identified the 17° domains as the most abundant ones followed by 13° domains [13]. Most frequently, $Ni_2C$ on
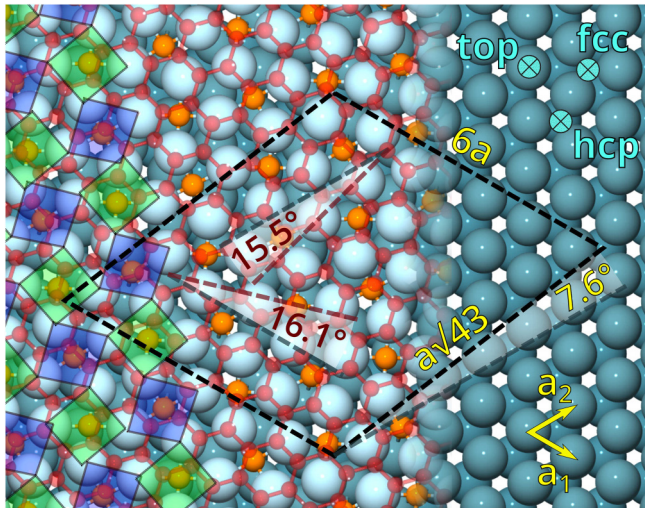
FIG. 1. RGC structure modeled with $(6 \times \sqrt{43}) R 7.6°$ unit cell depicted with thick black dashed lines. C atoms of G ($Ni_2C$) are represented by small transparent red spheres (orange spheres). Ni atoms of $Ni_2C$ (Ni(111)) are represented by big light blue (dark blue) spheres. Clock reconstruction of carbide is emphasized by green and violet squares. Ni(111) lattice in the bottom is revealed on the right by removing G and $Ni_2C$ from the image. Lattice vectors $\mathbf{a}_1$ and $\mathbf{a}_2$ that define the ⟨110⟩ directions of nickel lattice are depicted in the lower right corner, and adsorption sites on the nickel surface are labeled in the upper right corner. G rotation angles, measured between its zigzag directions and ⟨110⟩ directions of Ni(111), are labeled in the middle.

Ni(111) surface is modeled with quasi-square $\sqrt{39} R 16.1° \times \sqrt{39} \bar{R} 16.1°$ structure, where the denoted angles describe the orientation of the unit cell vectors with respect to ⟨110⟩ nickel surface directions and $\bar{R}$ denotes rotation in the opposite sense to $R$ [9,33]. This structure is described already in the pioneering work of McCaroll *et al.* [34], though recent studies argue that the stability of $\sqrt{39} R 16.1° \times \sqrt{37} \bar{R} 34.7°$ structure is slightly higher [11,35].

Given that G and Ni(111) surface share the same hexagonal lattice with small difference in lattice constants, any unit cell of $Ni_2C$/Ni(111) interface can readily accommodate the epitaxial graphene and thus can be used to model EGC structure. On the other hand, when G is rotated, the problem of accommodating three different lattices arises and unfortunately neither of the two aforementioned supercells is able to accommodate G rotated by 17° or 13° or by any angle close to it. To the best of our knowledge, nobody afforded the problem of accommodation of these three lattices before. To tackle it, we kept the Ni(111) lattice fixed and, by varying the structural parameters within $\pm 3\%$ compared to their equilibrium values, simultaneously accommodated $Ni_2C$ and G lattices. The details behind the construction procedure are provided in Ref. [17].

Our model of RGC structure is presented in Fig. 1. Among the inspected supercell candidates, we found the $(6 \times \sqrt{43}) R 7.6°$ to be the minimal one that is suitable to match three different lattices. Furthermore, it closely resembles the experimentally detected $Ni_2C$ structure [9] while still being computationally affordable. We used 18 C and 36 Ni atoms to

build $Ni_2C$ monolayer, whilst the bulk Ni below is modeled with two layers of Ni(111) containing 42 Ni atoms per layer. EGC heterostructure is modeled with the same supercell, with G adsorbed in the top-fcc configuration (see Fig. S2 of Ref. [17]). Yet, as an aftermath of the geometric constraints imposed by the shape of the $(6 \times \sqrt{43}) R 7.6°$ supercell, the number of graphene C atoms differs in two structures—the G layer contains 84 C atoms in EGC and 88 C atoms in RGC. In total, the EGC and RGC structures encompass 222 and 226 atoms, respectively. The graphene lattice constant in EGC is 1.2% larger as compared to the value of pristine G to satisfy the alignment condition with Ni(111). On the other hand, the shape of the supercell causes small shear strain in G of RGC. Consequently, the angles between zigzag directions of graphene and ⟨110⟩ directions of nickel are not equal, 15.5° and 16.1°, as depicted in Fig. 1.

Now we focus on the structural properties and energetics of EGC and RGC structures. After the structures are fully relaxed, the distance between G and carbide in EGC and RGC is 2.97 and 3.02 Å, respectively. For comparison, we found that the height of G adsorbed on Ni(111) in the top-fcc configuration is 2.10 Å, in agreement with the values reported in previous studies of G adsorption on Ni(111) [26]. The total energies of the two structures cannot be directly compared due to different number of atoms they contain. Therefore, to quantify the influence of G orientation on the structural stability, we calculated the G adsorption energy per C atom ($E_{ads}$) in EGC and RGC structures. In both cases, the $E_{ads} = -0.10$ eV is obtained, which is substantially lower than $-0.17$ eV we found for G adsorption on Ni(111) in top-fcc configuration and already reported in Ref. [26]. This is in agreement with the previous studies, where a weak graphene-nickel interaction is reported in cases where $Ni_2C$ is present at the nickel surface [11]. Additionally, we found that the change in G orientation does not affect the stability of G/$Ni_2C$/Ni(111) heterostructure, i.e. the $E_{ads}$ is the same in EGC and RGC structures. Hence, contrary to G adsorption on Ni(111) where both features of chemisorption and physisorption occur [28], modest $E_{ads}$ and sizable increase in graphene-metal distance suggest that G adsorption on $Ni_2C$/Ni(111) substrate can be undoubtedly characterized as a weak physisorption. In the end, since EGC and RGC structures are equally stable, we cannot explain why carbide formation occurs exclusively under RG domains by inspecting the energetic properties of these structures. Therefore the broader investigation that will include the structures that precede carbide heterostructures is needed. This will be afforded in Sec. III B.

### 2. C 1s core-level shifts as carbide fingerprints

In previous experimental studies of G on Ni(111) surface, the laterally resolved x-ray photoemission electron spectroscopy measurements (XPEEM) are used to identify different carbon species [12,13]. Given that carbon atoms in different domains have distinct chemical environments, the sensitivity of the binding energy (BE) of C 1s core electrons to changes in the coordination of neighboring atoms, i.e., core-level shifts (CLS), can be used as domain fingerprints [13]. The C 1s spectra in Ref. [13] of different graphene phases on Ni(111) were deconvoluted into four components, attributed

TABLE I. Comparison of calculated and experimental binding energies [12,13] of different carbon species on Ni(111) surface. DFT-calculated and the values obtained from the experiments are aligned with respect to the experimental BE of free graphene, 284.4 eV.

| Calculated BE (eV) | | Experimental BE (eV) | |
|---|---|---|---|
| Carbide C1 | 283.2 | Carbide | 283.2 |
| Carbide C2 | 283.6 | Dissolved C | 283.8 |
| EG (fcc, top) | 284.8, 284.9 | EG | 284.8 |

to EG, weakly interacting graphene (like G in RGC), carbide, and interstitial carbon dissolved into nickel. We report the BE obtained from DFT calculations and suggest a possible identification of the contributions to the XPS spectra in Ref. [13], making a comparison with the previous attribution.

The results are reported in Table I and schematically depicted in Fig. 2(b). The BE of free-standing graphene (284.4 eV) is taken as a reference. The calculated BE of carbon atoms in G above carbide is equal to the free-standing G, thus confirming once again that G is decoupled from the substrate. Most often, in the experimentally obtained BE of carbon structures on Ni(111), the reference peak is the one ascribed to EG as it has the highest intensity. However, two sublattices of EG have distinct coordination, and whereas the difference in BE of C atoms bound in top and fcc sites is not easy to distinguish experimentally, DFT calculations reveal small difference of around ∼0.1 eV. We obtained values of 284.8 and 284.9 eV for fcc and top C atoms, respectively, in excellent agreement with the experimental value for EG of 284.8 eV [13].
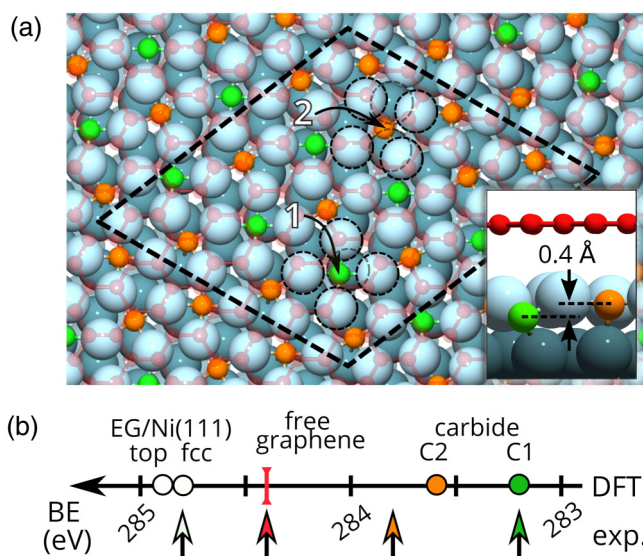


FIG. 2. (a) Two different coordinations of carbon atoms in Ni$_2$C. C atoms represented by green (orange) spheres and labeled by 1 (2) have fivefold (sixfold) coordination of Ni atoms. In the inset the side view of a portion of Ni$_2$C structure is presented, emphasizing different heights of C1 and C2 atoms; (b) schematic representation of core electron binding energies (in eV) for different carbon species. Experimental values are taken from Ref. [13].
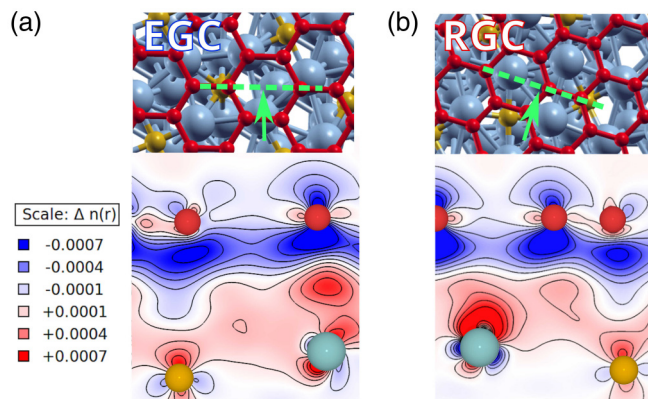


FIG. 3. Charge density induced (ICD) upon G adsorption at Ni$_2$C/Ni(111) interface in epitaxial (a) and rotated (b) configuration. The planes used to plot ICD are denoted by dashed green lines in the upper panels and the view directions by green arrows. C atoms of G (Ni$_2$C) are represented by small red (orange) spheres, and Ni atoms by larger light blue spheres. The thermographic scale on the left is in electrons/Bohr$^3$ and stands for both images.

Close examination of carbon atoms in Ni$_2$C shows that they display two different coordinations, as depicted in Fig. 2(a). In particular, 1/3 of carbide C atoms, represented by green spheres (C1), are surrounded by four Ni atoms laying in the same plane and have one Ni atom underneath, which makes their coordination fivefold. For C1, we obtained the BE of 283.2 eV which perfectly matches the experimentally measured BE ascribed to carbide structure (Table I). On the other hand, 2/3 of carbide C atoms, represented by orange spheres (C2), are adsorbed in bridge site above the two Ni atoms of the first Ni(111) layer. Thus, their coordination is sixfold and we obtained BE of 283.6 eV for C2 atoms.

The BE of carbon atoms dissolved in the first few subsurface Ni(111) layers reported in Ref. [13] is 283.8 eV, very close to the value we obtained for C2 atoms. Therefore we suggest that the peak attributed in Ref. [13] to dissolved C could be alternatively attributed to (or could contain a contribution from) the C2 atoms of carbide. Its very low intensity can be explained by structural arguments, as C2 atoms are 0.4 Å deeper than C1 atoms [see inset in Fig. 2(a)]. Thus they are at the very end of the reach of photoelectrons whose effective attenuation length is reported to be ∼4.4 Å [13]. Apart from this detail that would require further investigation, the overall agreement between the calculated and the experimentally obtained BE values is a firm support for our computational models of carbide structures.

### 3. Other electronic properties of carbide structures

To reveal how the change in G orientation affects its electronic structure, we calculated the charge density induced (ICD) upon the G adsorption on Ni$_2$C/Ni(111) substrate (Fig. 3). From ICD plots small electronic charge transfer of similar magnitude from G to Ni$_2$C has been found both in EGC and RGC. Löwdin population analysis of valence charge projected on atomic orbitals showed that C atoms of graphene lose 0.05 electrons irrespective of G orientation, while the mean value of electronic charge gained on Ni atoms of carbide is 0.06 electrons. Changes in charge of C atoms in carbide are
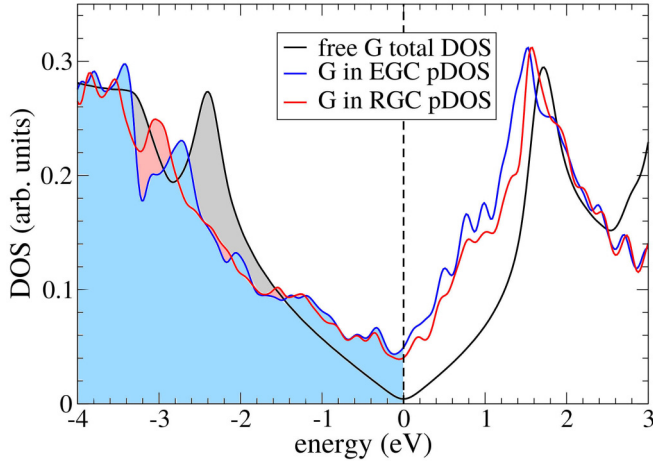
FIG. 4. Atomic projected density of states of $s$ and $p$ orbitals (pDOS) averaged over the C atoms of G in EGC and RGC structures, and total DOS of free-standing G. Fermi levels of the corresponding structures are aligned to zero of the energy scale.

even smaller and do not exceed 0.02 electrons. Thus, by supporting the ICD plots with the results from Löwdin analysis, we conclude that the small portion of electrons transferred from graphene to Ni$_2$C is redistributed mainly between the Ni atoms of Ni$_2$C. The charge of Ni atoms in Ni(111) is unaffected by graphene adsorption.

As reported in Ref. [13], microprobe angle-resolved photoelectron spectroscopy ($\mu$-ARPES) measurements performed on RGC domains clearly show the Dirac cone (DC), a feature distinctive of free-standing G, lying very close to $E_F$. To expose the influence of G orientation on the position of DC, we compared the atomic projected density of states (pDOS) of G in EGC and RGC to total DOS of free-standing G, as depicted in Fig. 4.

Despite the fact that DC cannot be easily located in Fig. 4 because pDOS calculations require very dense **k** grid to smooth the numerical oscillations, from the plot can be rationalized that the DC in both EGC and RGC heterostructures is located within a ~0.1 eV interval around $E_F$. The higher DOS near $E_F$ of EGC and RGC as compared to free-standing G includes the contribution from $p$ states of carbide C atoms in the projections. The appearance of DC at the energies close to $E_F$ is a clear fingerprint of free-standing G which proves that its semimetallic nature is completely restored upon the formation of carbide on Ni(111) surface, while the striking similarity between the pDOS of G in EGC and RGC indicates that the change in G orientation does not affect its electronic properties.

### B. Towards carbide formation at G/Ni(111) interfaces

The reconstruction of nickel surface upon exposure to hydrocarbons is not distinctive only of fcc(111) surface. For instance, an increase in carbon concentration up to 0.5 monolayer (ML) on Ni(100) triggers the local displacement of Ni atoms which ends with the formation of an alternate arrangement of rhombi and squares [36]. Another example is the formation of carbide structure on Ni(110) surface, which is accompanied by a long-range mass transport of Ni atoms [37].

Experimental findings from this study suggest that carbon is most probably not embedded in the first Ni layer but must be subsurface. Both Ni(100) and Ni(110) examples imply that upon the increase in concentration of surface and/or subsurface C atoms the nickel surfaces become unstable, while it is evident that the type of the reconstruction and the critical C concentration needed to trigger the structural phase transition are highly dependent on the experimental conditions.

To examine the reconstruction of Ni(111) surface, we compared the relevant thermodynamic quantities of two structural phases: (1) the initial Ni(111) structure with added surface and/or subsurface C atoms and (2) the carbidic phase formed on Ni(111) surface. We assume that carbide C atoms are supplied from the subsurface $oh$ sites and calculate the carbide formation energy per Ni$_2$C unit as

$$\Delta E_f = \frac{1}{N}(E(\text{Ni}_2\text{C}/\text{Ni}(111)) - E(\text{Ni}(111))$$
$$- N \times E(\text{C}) - 2N \times E(\text{Ni}^{fcc})), \qquad (1)$$

where $E(\text{Ni}_2\text{C}/\text{Ni}(111))$ is the total energy of Ni$_2$C/Ni(111) structure and $N$ is the number of Ni$_2$C units in the supercell. Other terms are: $E(\text{Ni}(111))$ is the total energy of Ni(111) slab, $E(\text{C}) = E(\text{C}/\text{Ni}(111)) - E(\text{Ni}(111))$ is the total energy difference between the Ni(111) with one C atom in the subsurface $oh$ site and the total energy of pristine Ni(111), and the last term $E(\text{Ni}^{fcc})$ is the total energy of a Ni atom in the bulk $fcc$ crystal. The estimated formation energy is $\Delta E_f = -0.3$ eV. Together with the experimental evidence of surface carbide structures [9], this suggests that the preference for Ni$_2$C formation grows as the C concentration increases. However, the critical concentration of C atoms needed to trigger the structural phase transition and the role of G cover is still under debate. In this section we discuss the microscopic mechanisms leading to carbide formation under G and the necessity of G rotation for such process to happen.

#### 1. Influence of rotation on G binding to Ni(111)

Now we discuss how the G rotation affects its stability on Ni(111). Bearing in mind that carbon concentration plays a crucial role in carbide formation on Ni(111), we will explore the structural phase transition taking place under the EG and RG. Considering that a full carbide layer is not present in the structures which will be examined here, only two different lattices are to be matched: Ni(111) and G rotated with respect to $\langle 110 \rangle$ directions of nickel. Therefore, by applying the construction algorithm explained in Sec. III A 1 and in Ref. [17], we searched for the smallest possible cell able to accommodate G rotated by 17° or 13° chosen as the two most abundant angles among experimentally obtained RG domains. We found that the $(\sqrt{19} \times \sqrt{19}) R\, 23.4°$ cell is the most suitable candidate, able to accommodate G rotated by 13.2° (Fig. 5). By exploiting the fact that Ni(111) surface share the lattice with G, the rotation angle can be easily found if one notices that this supercell corresponds to linear combination of unit vectors $3\mathbf{a}_1 + 2\mathbf{a}_2$ and applies Eq. (2) from Ref. [38]. Modeled with $(\sqrt{19} \times \sqrt{19}) R\, 23.4°$ cell, both EG and RG structures contain 95 atoms—three layers of Ni(111) with 19 Ni atoms per layer and 38 C atoms of graphene. Furthermore, the STM images we obtained from
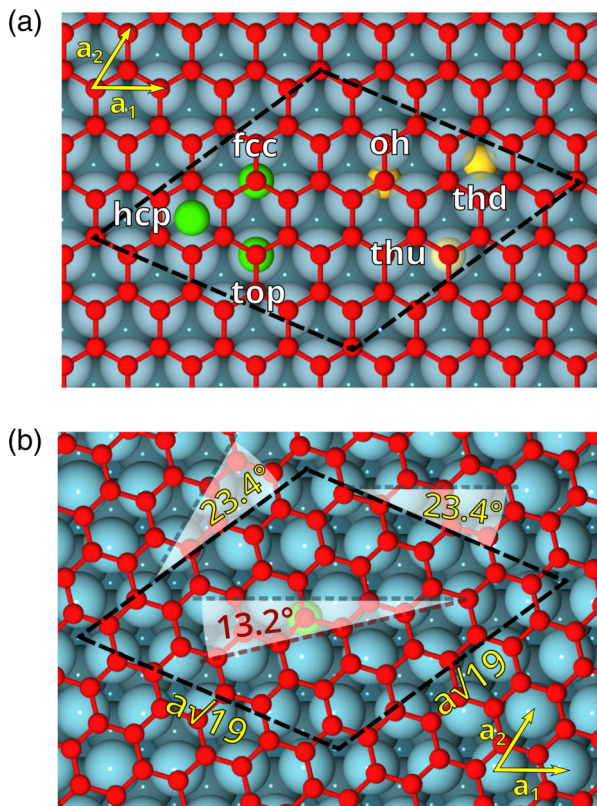
FIG. 5. Structural models of (a) EG and (b) RG made with $(\sqrt{19} \times \sqrt{19}) R \, 23.4°$ unit cell. In (a), the surface and the subsurface sites of EG are represented by green and gold spheres, respectively. In (b), the structural details of the unit cell are denoted, in particular: length of the unit cell vectors and the angles between them and $\langle 110 \rangle$ crystallographic directions of nickel. Ni(111) surface lattice vectors are depicted by yellow arrows. The G rotation angle, measured between the $\langle 110 \rangle$ nickel direction and the zigzag direction of G is 13.2°. Green sphere in the middle depicts the most stable surface site for binding C atom directly under RG.

DFT calculations (see Fig. S3 in Ref. [17]) are in excellent agreement with the experimental ones presented in Fig. S6 of Ref. [13] for G domains rotated by 13°.

Now we discuss how the G orientation affects its binding on Ni(111) and determines its stability. To clearly distinguish between the carbon atoms of G from those possibly at the G/Ni(111) interface, we label the former as $C_G$ and the latter will be simply called C atoms. Direct comparison of total energy of EG and RG structures yields the difference of 1.48 eV (0.04 eV/$C_G$ atom on average) in favor of EG. This is a clear indication that G prefers to align with Ni(111). We argue that the difference in total energy of EG and RG stems from different number of strong $C_G$-Ni bonds in two structures, i.e., from different number of $C_G$ atoms adsorbed in (or very near) *top* sites. As stated in Sec. III A 1 the most favorable EG adsorption geometry is top-fcc, where half of the $C_G$ atoms are on *top* of Ni atoms while the other half are above the *fcc* sites. Given that $C_G$ atoms residing in different sites do not contribute equally to the G adsorption energy, one can estimate their individual contributions by applying the following procedure. We assumed that $C_G$ atoms of EG

TABLE II. Binding energy $E_{\text{bind}}$ (in eV) of an individual C atom in different surface and subsurface substrate sites of pristine Ni(111), and at EG and RG interfaces. The dashes (-) indicate unstable binding sites and the stars (*) denote the values averaged over *fcc*- and *hcp*-like sites under RG.

| System | top | fcc | hcp |
|---|---|---|---|
| Ni(111) | – | 6.90 | 6.96 |
| EG | 2.69 | 5.30 | – |
| RG | – | 5.99* | 6.12* |
| | *oh* | *thu* | *thd* |
| Ni(111) | 7.46 | 6.41 | – |
| EG | 7.18 | 5.98 | 5.52 |
| RG | 7.39 | – | – |

can reside in one of those three sites: top, fcc, and hcp. Then, using $1 \times 1$ unit cell with two $C_G$ atoms, we inspected three EG configurations, namely top-fcc, top-hcp, and fcc-hcp. EG configurations with $C_G$ atoms residing in bridge sites are not considered. For each configuration we calculated the adsorption energy of the two $C_G$ atoms. With a simple algebra, from three EG configurations we extracted adsorption energies of $C_G$ atoms at three different sites. Finally, we found that a single $C_G$ atom adsorbed in top, fcc, and hcp site contributes to the adsorption energy of G sheet by $-0.23$, $-0.11$, and $-0.08$ eV, respectively. The much larger contribution of *top* site as compared to the other two is a firm clue that the number of $C_G$ atoms sitting in *top* sites determines the stability of G/Ni(111) structure – the higher the number of occupied *top* sites, the greater the stability. We consider the $C_G$ atom of RG bounds in the *top* site if the distance between its projection on the Ni surface and the closest Ni atom is less than 0.5 Å. In our models of EG and RG structures depicted in Fig. 5, there are 19 and 8 $C_G$ atoms sitting in *top* sites, respectively. If we assume that $C_G$ atoms not bound in *top* sites are bound somewhere between *fcc* and *hcp* sites, as the rule of thumb the difference between the two contributions is $(19 - 8) \times (0.23 - (0.11 + 0.08)/2) = 1.49$ eV, which is roughly the difference in total energies of EG and RG structures.

### 2. Binding of an individual C atom at Ni(111) surface: Effects of G cover

We continue with the exploration of the effect that G cover has on the nickel reactivity by comparing the binding of an individual C atom on clean Ni(111) to those under EG and RG. We considered three surface sites—*top*, *fcc*, and *hcp*—and three subsurface sites between the second and the first Ni layer, namely: octahedral (*oh*), tetrahedral-up (*thu*), and tetrahedral-down (*thd*). Binding sites are depicted in Fig. 5(a). The corresponding binding energies ($E_{\text{bind}}$) are defined as

$$E_{\text{bind}} = E(\text{C}) + E(\text{Sup}) - E(\text{C/Sup}), \quad (2)$$

where $E(\text{C})$ is the total energy of the isolated C atom in a box, $E(\text{Sup})$ is the total energy of the support, i.e., Sup = {Ni(111), EG, RG}, and $E(\text{C/Sup})$ is the total energy of C atom bound to the support. The $E_{\text{bind}}$ values are presented in Table II.

C atom displays very strong binding on pristine Ni(111) surface, with $E_{bind}$ of 6.96 and 6.90 eV corresponding to hollow $hcp$ and $fcc$ sites. The highest $E_{bind}$ corresponding to hollow sites are also reported in the previous studies of carbon adsorption on the Ni(111) surface [39,40]. At variance with $C_G$ atoms of graphene, which prefer to bind to $top$ site, an individual C atom is unstable in $top$ site and relaxes to $hcp$ site, indicating that the formation of a single C-Ni bond is unfavorable. This suggests that the character of C-Ni bond crucially depends on the hybridization of C $2p$ orbitals. The overlap between the G $\pi$ orbitals, formed upon $sp^2$-hybridization, and the Ni $3d_{z^2}$ orbitals is essential for G stability on Ni(111) [28]. On the other hand, a single C atom, which lacks $sp^2$-hybridized orbitals, prefers to bind in sites with high Ni coordination. Similarly, a top-fcc G flake terminates with $C_G$ atoms in hollow rather than top sites [41].

Once the Ni(111) is covered with G, the $E_{bind}$ at the surface sites substantially decrease, indicating the strongly repulsive character of the interaction between the C atom and G cover (see Table II). This interaction combines geometric and electronic effects. The former gives rise to a marked difference in the $fcc$ and $hcp$ binding sites under G. To simplify the discussion we refer to binding of C atom on the free-standing G—the $E_{bind}$ at the hollow site (above the center of the G hexagon) is as much as 2.04 eV lower than the value corresponding to a C atom bound on top of a $C_G$ atom. Qualitatively, the same binding picture is found in G/Ni(111) interface. In EG interface, C atom that is bound in $hcp$ site directly below G hollow site is unstable and relaxes to subsurface $thd$ site [see Fig. 5(a)]. Contrarily, it is stable in $fcc$ site under $C_G$ atom although the $E_{bind}$ is greatly reduces compared to the value obtained for the same site of clean Ni(111). Considering C binding in RG [Fig. 5(b)], every Ni(111) surface site is unique due to distinctions in local coordination of $C_G$ atoms. Nonetheless, the geometric effect of G cover is present, as the only stable surface sites are Ni-threefold hollow sites with $C_G$ atom directly above them, such as the $hcp$-like site denoted by green sphere in the middle of Fig. 5(b).

Difference in C binding under EG from that under RG can be explained by electronic effect with a simple understanding offered by the $d$-band model of Hammer and Nørskov [42]. Here we will focus on two particular Ni-threefold hollow sites with a $C_G$ atom directly above it—(any) $fcc$ site under EG and $hcp$-like site under RG denoted in Fig. 5(b). DOS plot in Fig. 6 shows changes induced by G cover in the electronic properties of the surface Ni atoms surrounding these sites.

The Ni $3d$ states centers are at $-1.84$ and $-1.65$ eV with respect to Fermi levels of EG and RG structures. According to the $d$-band model, the pronounced electronic structure effect, quantified by a decrease in the $d$-band center values of surface Ni atoms, is expected to slightly reduce the reactivity of the metal surface when EG is compared to RG. Entirely in agreement with DFT calculations, the model predicts weaker C binding under EG (inset of Fig. 6). Finally, the combined geometric and electronic effects of G cover drastically reduce $E_{bind}$ of C atom as compared to pristine Ni(111) surface.

### 3. Binding of an individual C atom in Ni(111) subsurface

Now we describe C binding in subsurface, in particular between the second and the first Ni layer. Although the G cover
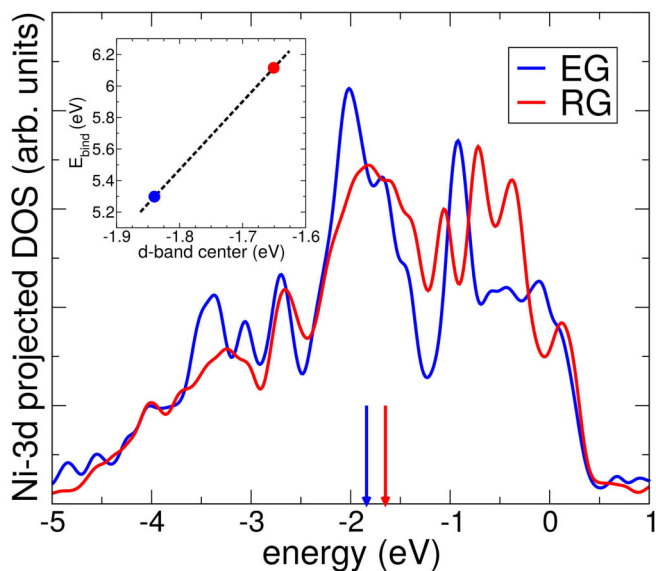


FIG. 6. Density of states (DOS) projected on $3d$ orbitals averaged over the Ni atoms nearest to C in the most stable surface sites under EG and RG cover. Arrows indicate the position of $d$-band center. The correlation between $E_{bind}$ of C atom and the position of $d$-band center is plotted in the inset. The Fermi energy is set to zero.

does not affect the subsurface C atoms as much as the ones on the surface, the importance of its alignment with nickel surface is observable in any process that is accompanied by displacements of surface Ni atoms.

Among three considered subsurface sites [see Fig. 5(a)], we found the $oh$ site by far the most favorable one. The high stability of C atom bound in $oh$ site originates from high Ni coordination, as it is surrounded by six Ni atoms at the distance of 1.86 Å. The $E_{bind}$ for $oh$ site in pristine Ni(111) and under EG and RG is 7.46, 7.18, and 7.39 eV, respectively. These values are much larger than the $E_{bind}$ for any surface site in the corresponding structures. The preference of subsurface over surface sites are in agreement with the previous studies of C adsorption on Ni(111) [40,43]. Here, we stress out that the binding of C atom to $oh$ site under EG is slightly weaker than in pristine Ni(111) or under RG. The reason behind this are $C_G$ atoms of EG which hold tight the Ni atoms underneath and hinder their displacement from the ideal fcc(111) positions. Therefore the unreleased stress of surface Ni atoms under EG cover reduces the binding of C atom in $oh$ site. To put it differently, EG causes *the locking* of the nickel surface.

To investigate the possibility of a C atom in $oh$ site to segregate to surface $fcc$ site under EG and RG, we used the NEB method to calculate the barriers (Fig. 7). The $fcc$ site is chosen as the only surface site stable both under EG and RG. The calculated barriers of 2.23 and 1.51 eV in EG and RG structures indicate that the segregation of a single C atom is very unlikely to occur as long as Ni(111) surface is intact, i.e., as long as Ni atoms remain in fcc(111) positions. On the other hand, much smaller barriers of 0.36 and 0.17 eV for dissolution, i.e., for the diffusion from $fcc$ to $oh$ site, suggest that the stability of C atom on the surface at room temperature is arguable.
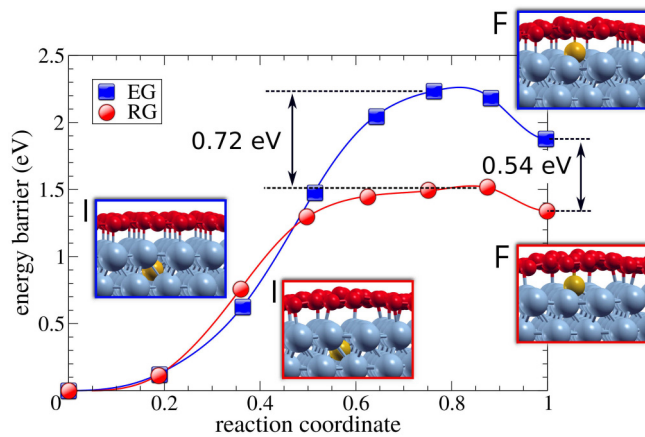
FIG. 7. Barriers for segregation of C atom from *oh* to *fcc* site under EG (blue squares) and RG (red circles) as calculated via NEB method. The initial and the final image of segregation under RG is depicted in the inset.

High barrier for surface segregation and low barrier for dissolution together with high $E_{bind}$ for shallowest *oh* sites indicate that an increase in subsurface C concentration is to be expected. Moreover, the higher barrier for segregation under EG can be explained by the fact that the migration of C atom to subsurface must be followed by local displacements of surface Ni atoms which are held tight by EG above. This is another consequence of locking of the nickel surface, which is of key importance for hindering the carbide formation under EG.

To rationalize the preference of C atoms to occupy bulk regions in nickel, we calculated $E_{bind}$ for *oh* sites between the third and the second Ni layer. These calculations were done with five Ni layers. In pristine Ni(111) and under RG, the $E_{bind}$ of C atom in bulk *oh* site is, respectively, 0.32 and 0.23 eV lower as compared to the subsurface *oh* site. In previous studies the lower binding energy of bulk interstitials, i.e., C atoms bound in voids deep inside the metal, as compared to the subsurface interstitials, is ascribed to an enhancement of the elastic response energy [43]. Indeed, the high Ni-coordination of subsurface sites equal to that of bulk sites leads to higher $E_{bind}$ than the values corresponding to the surface sites, while the ability of surface Ni atoms to displace and optimize the length of C-Ni bonds gives the preference to binding of C atoms in the subsurface.

Contrary to C binding in Ni(111) and RG structures, in EG we found no difference in $E_{bind}$ corresponding to *oh* sites of different depth. Similar finding is reported in Ref. [44], where the difference between the $E_{bind}$ of subsurface and subsubsurface C atom is only 0.1 eV for G-Ni distance of 2.0 Å. We explain the equal $E_{bind}$ corresponding to *oh* sites of different depth as another manifestation of locking of the nickel surface, as surface Ni atoms are unable to move and optimize the length of C-Ni bonds. Furthermore, this may be an indication that C atoms dissolved in bulk Ni in samples where both EG and RG domains are present upon segregation would prefer to increase their concentration in the subsurface regions under RG. However, to fully examine the C segregation in EG and RG domains, more advanced models of G/Ni(111) interfaces that would include the depth gradient of carbon concentra-
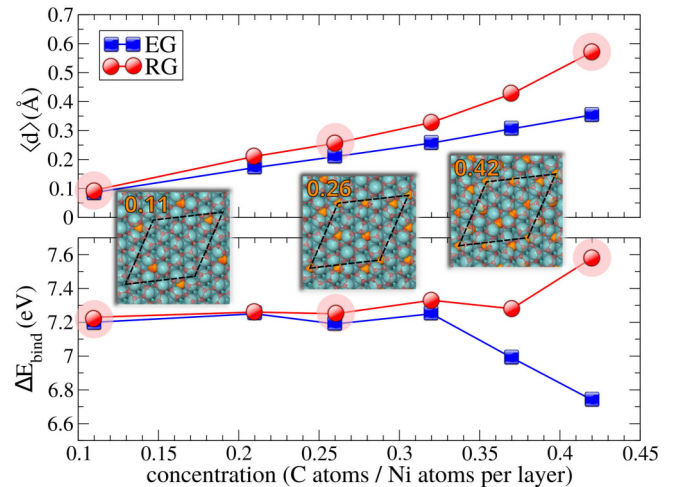


FIG. 8. The mean absolute displacement $\langle d \rangle$ of surface Ni atoms (top) and the incremental binding energy $\Delta E_{bind}$ for the addition of subsurface C atoms to *oh* sites (bottom) in EG (blue) and RG (red) at various concentrations $\Theta$. Top view of RG structures with $\Theta = 0.11$, 0.26, and 0.42 ML are presented in the middle, with the points in graph corresponding to these structures emphasized by semitransparent red circles.

tion must be considered, which is out of the scope of this work.

### 4. Increasing the concentration of subsurface C atoms under EG and RG

Experimental studies of carbide formation under RG suggest that C atoms, needed for this process, are supplied from inner layers. Upon cooling, the C atoms dissolved into bulk nickel segregate to surface [13]. This is a common trend when C is an impurity in materials, since its bulk solubility reduces with temperature [45]. The structural phase transition from C enriched Ni layers to carbide occurs when the critical concentration $\Theta_{crit}$ of subsurface carbon is reached. Here, we inspect how an increase in $\Theta$ affects the structural properties of Ni(111) layers near the surface, covered by EG and RG.

Following the preference of C atom to bind in subsurface *oh* site, we simulated the increase in the concentration of subsurface carbon in EG and RG structures by sequentially adding C atoms one-by-one to *oh* sites. Due to geometrical constraints imposed by the shape of the $(\sqrt{19} \times \sqrt{19}) R\, 23.4°$ unit cell, the structures with homogeneous coverage of subsurface C atoms cannot be realized for any concentration. Therefore first we put C atoms into mutually distant *oh* sites to suppress the C-C interaction and then we add the C atoms in the *oh* sites in between. To quantify the deformation of nickel surface upon carbon addition, we calculated the mean absolute displacement $\langle d \rangle$ of Ni atoms from the first layer from their initial positions in EG and RG, Fig. 8(a). Finally, as a measure of the energy gain upon carbon addition, we calculated the incremental binding energy $\Delta E_{bind}$ for every additional subsurface C atom put in G/Ni(111) interface, as shown in Fig. 8(b).

At low concentrations not exceeding $\Theta \sim 0.3$ ML in both structures, the mean nickel displacement is increasing

linearly with an increase in concentration, without substantial dislocation of Ni atoms from their initial positions. Also, $\Delta E_{bind}$ changes only slightly around the value obtained for the binding energy of an individual C atom. This indicates that at low $\Theta$ both in EG and RG the Ni(111) structure sustains carbon addition.

However, at $\Theta \sim 0.35$ ML, there is an opposite variation in $\Delta E_{bind}$ in two structures. In EG, the abrupt decrease in $\Delta E_{bind}$ suggests that further increase in carbon concentration becomes unfavorable. This is in a sharp contrast with the behavior in RG where the increase in $\Delta E_{bind}$ indicates extra energy gain for every additional subsurface C atom, i.e., the growing tendency of RG structure to increase the concentration of subsurface carbon. From the steep increase of mean displacement of surface Ni atoms under RG cover [Fig. 8(a)], we conclude that the critical concentration for triggering the phase transition is close to 0.35 ML. However, to precisely obtain the $\Theta_{crit,RG}$ one must use much larger supercell that allows finer $\Theta$ variations.

The physical mechanism behind the different trends observed for $\Delta E_{bind}$ in two structures originates from the locking of the nickel surface caused by EG cover. Under RG, already at $\Theta \sim 0.35$ ML the surface Ni atoms are noticeably dislocated from their fcc(111) positions. This manifestation of the ongoing phase transition is substantially different from the behavior observed under EG cover, where nickel surface is held tight under G due to a strong overlap of G $\pi$ and Ni $3d_{z^2}$ orbitals. Therefore it is much harder to displace surface Ni atoms in EG than in RG. Consequently, when nickel is covered with EG, the fcc(111) structure is still preserved at $\Theta \sim 0.4$ ML.

Within the inspected $\Theta$ interval in EG we did not observe structural manifestations of the ongoing phase transition. Moreover, the vast decrease of $\Delta E_{bind}$ under EG cover rationalized from Fig. 8(b) shows that at $\Theta > 0.35$ ML further addition of C atoms is very unfavorable. Together with the conclusions drawn from the inspection of C binding to *oh* sites of different depth (Sec. III B 3), this can explain the inability of C atoms to increase their concentration under EG up to the phase transition threshold. Finally, we argue that $\Theta_{crit,RG}$ should depend on G rotation angle, as the G misalignment determines the number of short $C_G$-Ni bonds and thus the extent to which the surface is locked, which is maximal under EG and gradually reduces as G is rotated.

## IV. CONCLUSIONS

Applying DFT calculations we studied the role of G cover on the reactivity of Ni(111) surface and microscopic mecha-

nisms for the $Ni_2C$ formation observed in recent experiments. Structural models of G/Ni(111) and G/$Ni_2C$/Ni(111) heterostructures were constructed and validated by comparison with available experimental data. In particular, the complex structural model for RGC shows a fair agreement between calculated C $1s$ core-level shift of different carbon species in G/$Ni_2C$/Ni(111) heterostructure and the corresponding measurements. We found a substantial weakening of additional C atoms binding at Ni(111) beneath the G layer which is rationalized by inspecting local surface Ni $3d$ electronic states and applying the $d$-band model. Furthermore, we proved that G cover even induces the destabilization of C adsorption sites at Ni(111) surface. For the restructuring of nickel surface and the formation of $Ni_2C$, the near-surface carbon density must increase up to a phase transition threshold. The epitaxially grown G completely locks the nickel surface, making progressively more difficult the C enrichment of Ni outermost layers, hindering the surface reconstruction and thus preventing the nickel carbide formation. When G cover is rotated with respect to Ni(111) surface, the C binding picture changes, the density of subsurface carbon can increase, reaching the critical concentration (estimated around 0.35 ML) which enables the structural transition of the C-enriched Ni(111) layer to a $Ni_2C$ monolayer. Our study explains why carbide is experimentally detected only under rotated G domains, suggesting the possibility of employing 2D covers to tune the metal surface reactivity and improve performance concerning target catalytic reactions.

[1] K. S. Novoselov, A. K. Geim, S. V. Morozov, D. Jiang, Y. Zhang, S. V. Dubonos, I. V. Grigorieva, and A. A. Firsov, Science **306**, 666 (2004).

[2] A. K. Geim and K. S. Novoselov, Nat. Mater. **6**, 183 (2007).

[3] X. Li, W. Cai, J. An, S. Kim, J. Nah, D. Yang, R. Piner, A. Velamakanni, I. Jung, E. Tutuc *et al.*, Science **324**, 1312 (2009).

[4] S. Bae, H. Kim, Y. Lee, X. Xu, J. Park, Y. Zheng, J. Balakrishnan, T. Lei, H. R. Kim, Y. I. Song *et al.*, Nat. Nanotechnol. **5**, 574 (2010).

[5] Q. Yu, J. Lian, S. Siriponglert, H. Li, Y. P. Chen, and S. Pei, Appl. Phys. Lett. **93**, 113103 (2008).

[6] R. S. Weatherup, B. C. Bayer, R. Blume, C. Ducati, C. Baehtz, R. Schlögl, and S. Hofmann, Nano Lett. **11**, 4154 (2011).

[7] A. Dahal and M. Batzill, Nanoscale **6**, 2548 (2014).

[8] D. E. Gardin, J. D. Batteas, M. A. Van Hove, and G. A. Somorjai, Surf. Sci. **296**, 25 (1993).

[9] C. Klink, I. Stensgaard, F. Besenbacher, and E. Lægsgaard, Surf. Sci. **342**, 250 (1995).

[10] H. Nakano, J. Ogawa, and J. Nakamura, Surf. Sci. **514**, 256 (2002).

[11] P. Jacobson, B. Stöger, A. Garhofer, G. S. Parkinson, M. Schmid, R. Caudillo, F. Mittendorfer, J. Redinger, and U. Diebold, ACS Nano **6**, 3564 (2012).

[12] L. L. Patera, C. Africh, R. S. Weatherup, R. Blume, S. Bhardwaj, C. Castellarin-Cudia, A. Knop-Gericke, R. Schloegl, G. Comelli, S. Hofmann *et al.*, ACS Nano **7**, 7901 (2013).

[13] C. Africh, C. Cepek, L. L. Patera, G. Zamborlini, P. Genoni, T. O. Menteş, A. Sala, A. Locatelli, and G. Comelli, Sci. Rep. **6**, 19734 (2016).

[14] P. Giannozzi, S. Baroni, N. Bonini, M. Calandra, R. Car, C. Cavazzoni, D. Ceresoli, G. L. Chiarotti, M. Cococcioni, I. Dabo *et al.*, J. Phys. Condens. Matter **21**, 395502 (2009).

[15] P. Giannozzi, O. Andreussi, T. Brumme, O. Bunau, M. B. Nardelli, M. Calandra, R. Car, C. Cavazzoni, D. Ceresoli, M. Cococcioni *et al.*, J. Phys. Condens. Matter **29**, 465901 (2017).

[16] J. P. Perdew, K. Burke, and M. Ernzerhof, Phys. Rev. Lett. **77**, 3865 (1996).

[17] See Supplemental Material at http://link.aps.org/supplemental/10.1103/PhysRevMaterials.5.014003 for the construction procedure of the $(6 \times \sqrt{43}) R \, 7.6°$ supercell, STM images of RG structure, and C $1s$ pseudopotential generation.

[18] S. Grimme, J. Comput. Chem **27**, 1787 (2006).

[19] P. Haas, F. Tran, and P. Blaha, Phys. Rev. B **79**, 085104 (2009).

[20] H. J. Monkhorst and J. D. Pack, Phys. Rev. B **13**, 5188 (1976).

[21] N. Marzari, D. Vanderbilt, A. De Vita, and M. C. Payne, Phys. Rev. Lett. **82**, 3296 (1999).

[22] S. R. Bahn and K. W. Jacobsen, Comput. Sci. Eng. **4**, 56 (2002).

[23] A. H. Larsen, J. J. Mortensen, J. Blomqvist, I. E. Castelli, R. Christensen, M. Dułak, J. Friis, M. N. Groves, B. Hammer, C. Hargus *et al.*, J. Phys. Condens. Matter **29**, 273002 (2017).

[24] A. Kokalj, J. Mol. Graph. Model. **17**, 176 (1999).

[25] S. M. Kozlov, F. Viñes, and A. Görling, J. Phys. Chem. C **116**, 7360 (2012).

[26] F. Bianchini, L. L. Patera, M. Peressi, C. Africh, and G. Comelli, J. Phys. Chem. Lett. **5**, 467 (2014).

[27] M. Fuentes-Cabrera, M. I. Baskes, A. V. Melechko, and M. L. Simpson, Phys. Rev. B **77**, 035405 (2008).

[28] F. Mittendorfer, A. Garhofer, J. Redinger, J. Klimes, J. Harl, and G. Kresse, Phys. Rev. B **84**, 201401(R) (2011).

[29] R. Zhao, J. Wang, M. Yang, Z. Liu, and Z. Liu, J. Phys. Chem. C **116**, 21098 (2012).

[30] X. Sun, S. Entani, Y. Yamauchi, A. Pratt, and M. Kurahashi, J. Appl. Phys **114**, 143713 (2013).

[31] Y. Gamo, A. Nagashima, M. Wakabayashi, M. Terai, and C. Oshima, Surf. Sci. **374**, 61 (1997).

[32] J. Lahiri, Y. Lin, P. Bozkurt, I. I. Oleynik, and M. Batzill, Nat. Nanotechnol. **5**, 326 (2010).

[33] R. Martinez-Gordillo, C. Varvenne, H. Amara, and C. Bichara, Phys. Rev. B **97**, 205431 (2018).

[34] J. J. McCarroll, T. Edmonds, and R. C. Pitkethly, Nature (London) **223**, 1260 (1969).

[35] R. Rameshan, V. Vonk, D. Franz, J. Drnec, S. Penner, A. Garhofer, F. Mittendorfer, A. Stierle, and B. Klötzer, Sci. Rep. **8**, 2662 (2018).

[36] C. Klink, L. Olesen, F. Besenbacher, I. Stensgaard, E. Laegsgaard, and N. D. Lang, Phys. Rev. Lett. **71**, 4350 (1993).

[37] C. Klink, I. Stensgaard, F. Besenbacher, and E. Laegsgaard, Surf. Sci. **360**, 171 (1996)

[38] P. Moon and M. Koshino, Phys. Rev. B **85**, 195458 (2012).

[39] D. J. Klinke, S. Wilke, L. J. Broadbelt, J. Catal. **178**, 540 (1998).

[40] H. Amara, C. Bichara, and F. Ducastelle, Phys. Rev. B **73**, 113404 (2006).

[41] L. L. Patera, F. Bianchini, G. Troiano, C. Dri, C. Cepek, M. Peressi, C. Africh, and G. Comelli, Nano Lett. **15**, 56 (2015).

[42] B. Hammer and J. K. Nørskov, Adv. Catal. **45**, 71 (2000).

[43] O. V. Yazyev and A. Pasquarello, Phys. Rev. Lett. **100**, 156102 (2008).

[44] R. S. Weatherup, H. A. Amara, R. Blume, B. Dlubak, B. C. Bayer, M. Diarra, M. Bahri, A. Cabrero-Vilatela, S. Caneva, P. R. Kidambi, M. Martin, C. Deranlot, P. Seneor, R. Schloegl, F. Ducastelle, C. Bichara, and S. Hofmann, J. Am. Chem. Soc. **136**, 13698 (2014).

[45] K. F. McCarty, P. J. Feibelman, E. Loginova, and N. C. Bartelt, Carbon **47**, 1806 (2009).